AFRL-AFOSR-VA-TR-2019-0167

Nanochemical Strategies for Propulsion Enhancement

Scott Anderson
UNIVERSITY OF UTAH SALT LAKE CITY

05/21/2019
Final Report

Air Force Research Laboratory
AF Office Of Scientific Research (AFOSR)/ RTB2
Arlington, Virginia 22203
Air Force Materiel Command

DISTRIBUTION A: Distribution approved for public release.

REPORT DOCUMENTATION PAGE

Form Approved
OMB No. 0704-0188

1. REPORT DATE (DD-MM-YYYY)	2. REPORT TYPE	3. DATES COVERED (From - To)
24-06-2019	Final Performance	15 Mar 2016 to 14 Mar 2019

4. TITLE AND SUBTITLE
Nanochemical Strategies for Propulsion Enhancement

5a. CONTRACT NUMBER

5b. GRANT NUMBER
FA9550-16-1-0141

5c. PROGRAM ELEMENT NUMBER
61102F

6. AUTHOR(S)
Scott Anderson

5d. PROJECT NUMBER

5e. TASK NUMBER

5f. WORK UNIT NUMBER

7. PERFORMING ORGANIZATION NAME(S) AND ADDRESS(ES)
UNIVERSITY OF UTAH SALT LAKE CITY
201 PRESIDENTS CIR RM 408
SALT LAKE CITY, UT 84112-9023 US

8. PERFORMING ORGANIZATION REPORT NUMBER

9. SPONSORING/MONITORING AGENCY NAME(S) AND ADDRESS(ES)
AF Office of Scientific Research
875 N. Randolph St. Room 3112
Arlington, VA 22203

10. SPONSOR/MONITOR'S ACRONYM(S)
AFRL/AFOSR RTB2

11. SPONSOR/MONITOR'S REPORT NUMBER(S)
AFRL-AFOSR-VA-TR-2019-0167

12. DISTRIBUTION/AVAILABILITY STATEMENT
A DISTRIBUTION UNLIMITED: PB Public Release

13. SUPPLEMENTARY NOTES

14. ABSTRACT
A four PI team (PI: Scott Anderson, Utah, co-PIs Anastassia Alexandrova, UCLA, James Dumesic and Manos Mavrikakis, U. Wisc.) developed alloy nanoparticle and sub-nano cluster catalysts for selective alkane dehydrogenation, with the goal of reducing coking tendency in endothermic cooling applications. In each thrust, theory and experiment were combined to predict and evaluate different alloys. Pt-Sn, Pt-Zn, and Pt-Ge alloys all showed promising activity and stability. Unwanted deep dehydrogenation to coke precursors was suppressed, and catalyst activity and lifetime was enhanced.

15. SUBJECT TERMS
Catalysis, Endothermic fuel

16. SECURITY CLASSIFICATION OF:			17. LIMITATION OF ABSTRACT	18. NUMBER OF PAGES	19a. NAME OF RESPONSIBLE PERSON
a. REPORT	b. ABSTRACT	c. THIS PAGE			BERMAN, MICHAEL
Unclassified	Unclassified	Unclassified	UU		19b. TELEPHONE NUMBER (Include area code) 703-696-7781

Standard Form 298 (Rev. 8/98)
Prescribed by ANSI Std. Z39.18

Final Report for AFOSR Project Grant No. FA9550-16-1-0141

Nanochemical Strategies for Propulsion Enhancement

PI: Scott L. Anderson, University of Utah

Co-PIs: Manos Mavrikakis and James A. Dumesic, University of Wisconsin-Madison, and Anastassia N. Alexandrova, University of California, Los Angeles

The primary goal of this team project was to develop strategies to enhance endothermic fuel cooling for hypersonics using catalysis. Our focus has been on alloy nanoparticle and sub-nano cluster catalysts, tuning selectivity, activity, and durability by varying the alloy. Two members of the team, Mavrikakis and Dumesic, focused on catalysts consisting of 3-5 nm particles dispersed on high surface area supports, such as silica or alumina. Mavrikakis did theory, guiding choice of alloying systems, and aiding interpretation and microkinetic modeling of the catalysts. Dumesic prepared and evaluated catalysts under realistic conditions. Alexandrova and Anderson focused on sub-nano cluster catalysts, and carried out tightly coupled theory and experiments on size-selected alloy catalysts in order to elucidate the catalytic mechanisms in greater detail, thus guiding refinement of the catalysts, and in some cases, development of new strategies.

A secondary goal of this project was to synthesize, characterize, and do ignition/combustion testing of energetic boron and aluminum nanoparticles. This portion of the work was carried out by Anderson, in collaboration with AFRL groups at Edwards AFB and Wright-Patterson AFB, and an academic group at McGill University and University of Alabama.

After a brief outline of the main focus of the team's efforts, to lay out the interconnections and synergy between the team's thrusts, detailed summaries are presented of the work. These summaries are grouped into Nanocatalysts (Mavrikakis and Dumesic) and Sub-nano catalysts (Alexandrova and Anderson). The energetic nanoparticle work is described at the end.

The work was tied together by the common goal of developing improved catalysts for endothermic fuel cooling, and therefore there was substantial overlap in the systems studied and synergies in terms of the kinds of information that was extracted from each type of theory or experiment. We focused on dehydrogenation as the endothermic reaction, rather than cracking. As Gorte recently showed,[1] alkane cracking can be less endothermic than expected (or even exothermic!) due to formation of aromatics which, at high conversion, tend to couple to form higher molecular weight products, which also tend to be coke precursors. Dehydrogenation of a model alkane (ethane) was adopted team-wide, because it is both theoretically and experimentally tractable. Pt alloy catalysts were the target systems. Pt would be undesirable in an industrial context, however, the amount of catalyst required for cooling applications is quite small, thus metals cost is not a serious consideration.

In the context of endothermic cooling, the desirable catalyst properties are high activity for alkane dehydrogenation to alkenes, but low activity for further ("deep") dehydrogenation to alkynes, alkylidenes or other coke precursors. Two potential strategies here are: 1. Weaken the alkene-catalyst binding energy, so that alkene products desorb quickly after formation, rather than remaining on the surface to undergo deep dehydrogenation, or 2. Design binding sites that are unable to catalyze dehydrogenation beyond alkenes for electronic, steric, or other reasons. Another important aspect of the problem is to stabilize the catalyst particles or clusters, to inhibit deactivation by sintering, which might occur by Ostwald ripening or cluster diffusion and agglomeration. For this purpose, it is desirable to increase both the cohesive energy within the particles, and to anchor them to the support. Examples of all these strategies were explored.

The theory work of Mavrikakis focused on surfaces of Pt with different atomic structure, and alloys of Pt with various metals, and also looked at the effects of selective poisoning of certain types of sites to enhance selectivity. Dumesic synthesized supported alloy nanoparticle catalysts for high pressure/high temperature catalysis experiments, studying selectivity, activity, and durability. In addition to ethane dehydrogenation, he studied the effects of co-feeds and of the reverse reactions, thus providing additional mechanistic information.

It was shown that for pure Pt, terrace sites have relatively low desorption energies for ethylene, compared to step sites, although in both cases the activation energy for deep dehydrogenation, forming coke precursors, was lower yet, i.e., coking is energetically favored. This is relevant to nanoparticles and clusters, because they have a high density of such low coordination sites. Decorating the more reactive step sites with alumina was predicted to improve coking resistance, and that was confirmed in experiments by Dumesic. Mavrikakis also surveyed free energy descriptors for a variety of alloys, looking for promising candidates, which were then studied in more detail, experimentally and theoretically.

Pt alloys with Sn and Zn were identified as especially promising. These increase the activation barriers to deep dehydrogenation to coke precursors, and lower the energy required to desorb ethylene, thus making the catalysts more selective for the desired alkane-to-alkene reaction. Dumesic prepared a variety of supported PtSn and PtZn alloy nanoparticle catalysts, and studied the ethane dehydrogenation reaction, showing substantially enhanced activity and stability with respect to deactivation. One observation of the dehydrogenation work was that methane was produced in the presence of co-fed H_2. To help understand the origin of the methane, a fundamental study of the reverse reaction – coupling methane to produce ethylene on PtSn catalysts – was also performed.

The theory of Alexandrova addressed sub-nano Pt alloy clusters supported on various oxides, focusing on fundamental issues relating to the evolution of cluster structures with increasing temperature

and reactant concentrations. She discovered dynamical effects leading to cluster size- and composition-specific reactivity and stability, and looked at Pt clusters alloyed or doped with both main group elements and metals. To address the dynamical nature of sub-nano supported clusters, Alexandrova developed new theoretical methods for identification of the structural ensembles of cluster catalysts present under reaction conditions, mapping the pathways for catalyst isomerization, simulating sintering, and building a new statistical mechanical paradigm to model such dynamic catalysis beyond traditional DFT.

Anderson had several tasks under this grant. The primary focus was on experiments on size- and composition-selected sub-nano cluster catalysts, including surface science characterization, studies of ethylene desorption vs. deep dehydrogenation, and *in situ* imaging by transmission electron microscopy (TEM) under high temperatures and pressures to 1 atm. This work focused on Pt, Pt-B and Pt-Sn alloy clusters, developing methods to make clusters with atomic control over both size and composition, using methods conceptually similar to those used in atomic layer deposition. Significant improvements in stability and coke resistance were observed, and theory by Alexandrova helped explain the mechanistic origin of the effects.

Anderson also had a task to prepare and do physical/spectroscopic characterization of high energy density boron and aluminum nanoparticles for use as additives to fuels and hypergolic propellants. This work was done in collaboration with several groups at AFRL/Edwards, AFRL/WPAFB, and McGill University, who carried out detailed theory, measured the effects of particle loading on propellant ignition and combustion, and measured particle energy content and thermal properties.

In the following, the results of the U Wisconsin team on nanocatalysts will be reported first, followed by the results of the Utah/UCLA team on sub-nano cluster catalysts. Finally, Anderson's work on energetic nanoparticles will be summarized.

I. Nanoparticle catalysis for alkane dehydrogenation

Manos Mavrikakis and James A. Dumesic

Department of Chemical & Biological Engineering, University of Wisconsin – Madison

A. Ethane Dehydrogenation on Pristine and AlO_x-Decorated Pt Stepped Surfaces

We studied the fundamental mechanistic aspects of ethane (C_2H_6) dehydrogenation on Pt catalysts to identify improved catalysts for endothermic cooling while minimizing coke formation. In particular, we calculated thermochemistry and activation energy barriers for the elementary steps in the C_2H_6 dehydrogenation reaction network on *pristine* Pt(433) terrace and Pt(433) stepped surfaces using plane-wave density functional theory (DFT). We demonstrated that C_2H_6 dehydrogenation to C_2H_4 is favored on the Pt(433) terrace, because C_2H_4 has a higher preference to desorb from that surface as opposed to undergo further dehydrogenation. We show in **Figure 1** the calculated potential energy diagram (PED) for ethane dehydrogenation on the terrace and step of Pt(433). As seen in **Figure 1(a)**, on the Pt(433) terrace, C_2H_6

can be dehydrogenated to C_2H_4, whereas further deep dehydrogenation reactions to C_2H_2 and CH_x fragments are more difficult compared to the Pt(433) step in **Figure 1(b)**. The facile deep dehydrogenation on the Pt step results in accumulation of coke precursors and thus poisoning/de-activation of the catalysts.[2-4]

As shown in the Pt(433) terrace potential energy diagram (PED) in **Figure 1(a)**, after the formation of adsorbed C_2H_4, there is a large desorption barrier of 1.34 eV in comparison to the 0.78 eV barrier to further dehydrogenate to form vinyl (CH_2-CH). Therefore, if C_2H_4* forms on the surface, then it will likely go through deep dehydrogenation and the surface is expected to be covered by coke precursor intermediates. Further dehydrogenation leads to C_2H_2, which can dehydrogenate, undergo C-C bond cleavage, or desorb to the gas phase with an energy barrier of 2.57 eV. For comparison, the PED of Pt(433) step is shown in the PED in **Figure 1(b)** where the C_2H_4 desorption barrier (1.73 eV) is even larger than on the Pt terrace and further dehydrogenation to form vinyl is hindered by a small barrier of 0.42 eV. Therefore, the under-

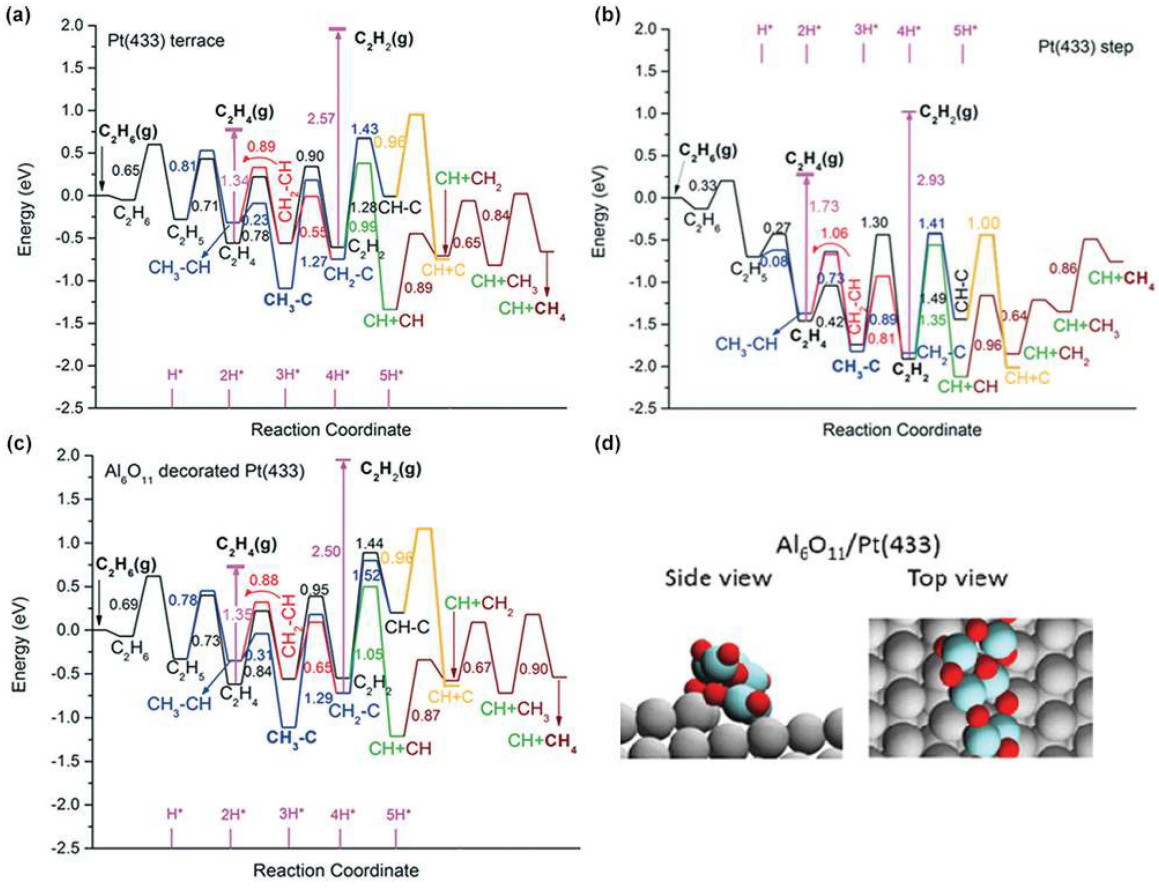

Figure 1: Potential energy diagram (PED) for C_2H_6 dehydrogenation on (a) Pt(433) terrace, (b) Pt(433) step, (c) Al_6O_{11}-decorated Pt(433) step-edge, and (d) cross section and top view of Al_6O_{11}-decorated Pt(433) step-edge. The total energies (at 0K) of the clean Pt(433) surface and gas phase C_2H_6 are used as the reference.

coordinated step sites on Pt(433) have an even higher preference for the deep dehydrogenation to C_2H_2 and CH_x fragments. Consequently, coke precursors accumulate on the surface especially at the step sites and result in deactivation of the catalyst. Based on these DFT results, our first approach was to see if we can at least partially mitigate coke formation on monometallic Pt nanoparticles by selectively deactivating the step sites by atomic layer deposited (ALD) alumina onto Pt nanoparticles.

It has been shown experimentally that atomic layer deposited (ALD) alumina can increase activity by decreasing coking and sintering for the oxidative dehydrogenation of ethane.[5] A few cycles of alumina ALD will selectively deposit preferentially onto low-coordination sites, effectively armoring the catalyst against coking. We calculated a PED of Al_6O_{11}/Pt(433)-step edge as shown in **Figure 1(c)**; structure shown in **Figure 1(d)**. For this armored surface, the PED for C_2H_6 dehydrogenation resembles that on the Pt(433) terrace (Fig. 1a). The desorption barrier of C_2H_4 is now comparable to the Pt(433) terrace (1.35 eV) with a further dehydrogenation barrier of 0.84 eV to form vinyl. Our modeling suggests that Al_6O_{11} decorated Pt(433) should be an effective method of armoring Pt nanoparticles against coking, at least by blocking the more prone to coke step sites of Pt nanoparticles.

To evaluate the hypothesis formulated on the basis of our DFT results for the effect of alumina overcoat on the reactivity of supported Pt catalysts for ethane (C_2H_6) dehydrogenation, we performed reaction kinetics experiments of ethane dehydrogenation on supported Pt catalysts, both pristine and ALD alumina overcoated. To assess the regenerability of our catalyst, we performed a series of experiments on the same catalyst sample, consisting of reduction–reaction–regeneration steps that were repeated consecutively. **Figure 2(a)** shows the measured ethylene Turn-Over-Frequency (TOF) as a function of time

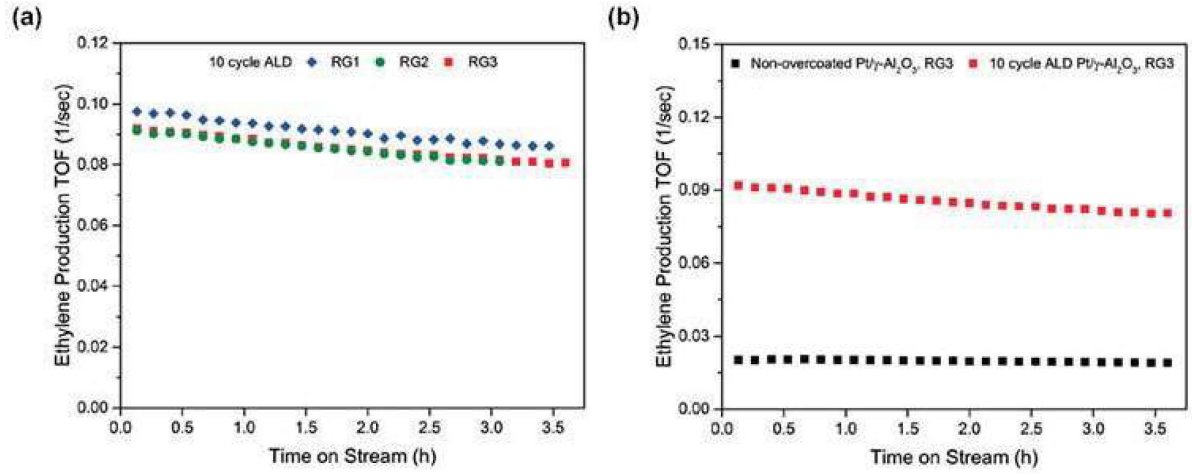

Figure 2: Ethylene production turn-over frequency (TOF) versus time on stream on (a) 10cALD/Pt/ γ-Al_2O_3 (after: one regeneration [RG1]; two regenerations [RG2]; three regenerations [RG3]) and (b) non-overcoated Pt/γ-Al_2O_3 and 10cALD/Pt/γ-Al_2O_3 catalysts after RG3. Reaction conditions: 873 K, 12.5 Torr ethane, 0 Torr hydrogen, and balance He for a total pressure of 1 atm.

on stream over a 10cALD/Pt/γ-Al2O3 catalyst (10 ALD cycles on the pristine Pt/ γ-Al2O3 catalyst) in a continuous flow reactor following the first, second, and third regenerations, respectively. The results shown in **Figure 2(a)** suggest that the catalyst activity is largely reversed upon calcination, indicating that the deactivation is primarily due to coking.

This regeneration-reduction-reaction cycle was also carried out for the non-overcoated Pt/γ-Al2O3 catalyst and a similar pattern was observed. Thus, both catalysts are stable and reusable over repeated calcination-reduction-reaction cycles. **Figure 2(b)** shows ethylene TOF versus time on stream for both catalysts after three regenerations. After 3 h on stream and in the absence of hydrogen, the 10cALD/Pt/γ-Al_2O_3 catalyst exhibited ~4 times higher ethylene TOF compared to the non-overcoated Pt/γ-Al_2O_3 catalyst.

B. Ethane dehydrogenation on Pt-Sn alloys

Another strategy we followed for reducing coke formation on Pt was to use Pt-based *bimetallic* catalysts. Oxophilic metals that can lower the d-band center of Pt and decrease the binding of CH_x species to Pt, make good candidates for alloying.[6] In particular, we studied a Pt_3Sn intermetallic using $Pt_3Sn(111)$ terrace and $Pt_3Sn(211)$ step surface as models for the DFT part of our work. The presence of Sn destabilized the binding of CH_x species on the surface and facilitated C_2H_4 desorption compared to pure Pt surfaces. The DFT calculated PED for $Pt_3Sn(211)$, step $Pt_3Sn(322)$, and terrace $Pt_3Sn(111)$ surfaces as shown in **Figure 3(a)**. After the C_2H_4* forms, it can either desorb as the desired product ethylene or go through deep dehydrogenation to form C_2H_3* and eventually coke leading to catalyst deactivation. For the $Pt_3Sn(111)$, further dehydrogenation is favored with an activation energy of 0.73 eV compared to the desorption energy of 0.92 eV. Compared to the PED for the terrace sites, the PED for the stepped alloy surfaces is shifted upwards. Therefore, on stepped Pt_3Sn surfaces, C_2H_4 is more likely to desorb than to be further dehydrogenated and form carbonaceous products. This behavior is in contrast to Pt step sites where the

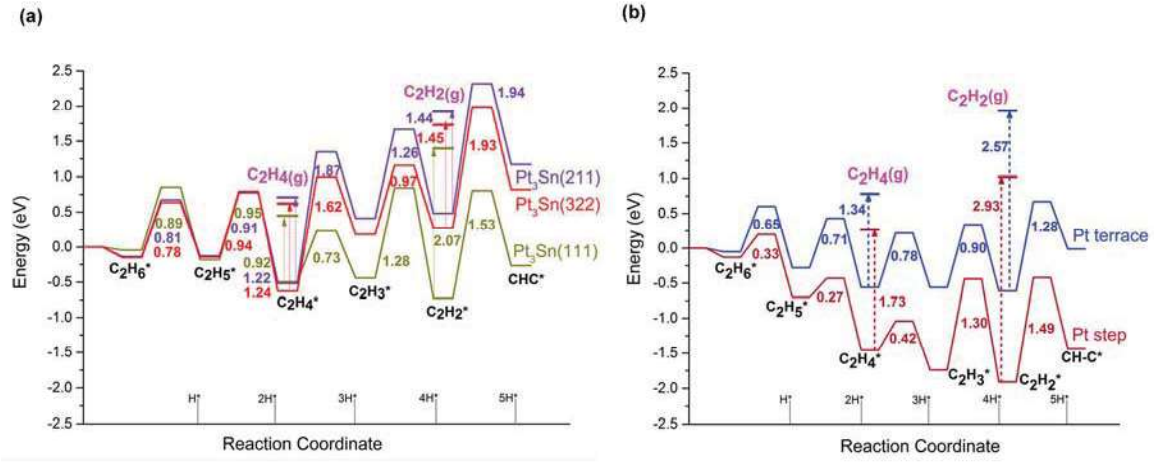

Figure 3: Calculated potential energy diagram (PED) for C_2H_6 dehydrogenation on: (a) $Pt_3Sn(211)$ step, $Pt_3Sn(322)$ step, and $Pt_3Sn(111)$ terrace, (b) Pt terrace compared to Pt step. The total energies calculated at 0 K of the clean surfaces and gas phase C_2H_6 are used as a reference.

PED for the Pt step site is shifted downward compared to Pt terrace (see **Figure 3(b)**), and, thus, the Pt step site is more likely to deactivate easier than the terrace site. Therefore, on Pt nanoparticles the goal is to decrease the reative fraction of step sites, which can be achieved by going to larger Pt nanoparticles, whereas the opposite is true for Pt_3Sn alloys, where one would pursue increasing the fraction of step sites by using smaller Pt_3Sn nanoparticles. These predictions can be further elucidated with microkinetic modeling.

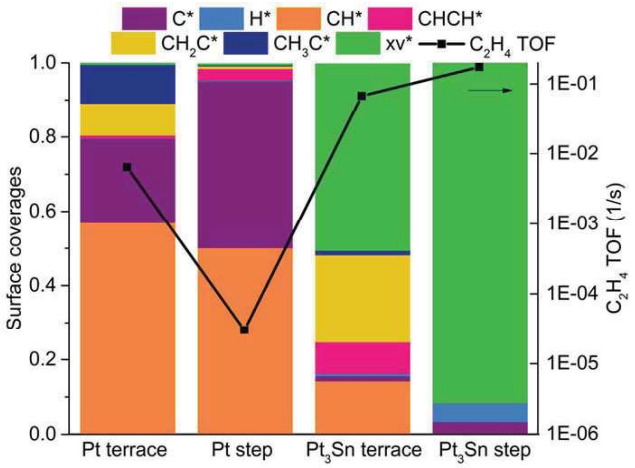

Figure 4: Surface coverages of various intermediates and ethylene TOF values of the studied surfaces predicted by the microkinetic model under reaction conditions of atmospheric pressure, 873 K, 12.5 Torr ethane pressure in the feed and 0 Torr H_2.

A microkinetic model of ethane dehydrogenation on Pt and Pt_3Sn surfaces was developed to gain insight into catalyst reactivity using DFT-derived parameters for terrace and stepped surfaces of Pt and Pt_3Sn. We used this model to predict the product formation rates and surface coverages of reaction intermediates under reaction conditions. The effect of: (i) Sn addition to Pt, (ii) varying C_2H_6 and H_2 pressures in the feed and (iii) reaction temperature were all investigated by comparing model predictions with experimental results. Adjustments to the DFT derived parameters were made to match experimentally determined quantities (reaction rates, orders, apparent activation energies, etc). The variations of surface coverages of intermediates and predicted C_2H_4 TOF values are shown in **Figure 4** for the case where hydrogen is not co-fed to the reactor. The microkinetic model predicts that both Pt_3Sn terrace and Pt_3Sn step sites contribute to the overall TOF of the catalyst with the Pt_3Sn step site being the most active. This behavior is in contrast to Pt catalysts where the majority of the activity comes from the Pt terrace site. In addition, the microkinetic model predicts that the Pt_3Sn sites are much less covered by intermediates compared to the Pt surfaces. The latter sites are predicted to be operating nearly full of surface intermediates.

Based on the microkinetic model calculations, both terrace and step surfaces of Pt_3Sn were predicted to have product formation rates and activation barrier trends in agreement with experimental observations, suggesting that ethane dehydrogenation reaction may *not* be particularly structure sensitive for Pt-Sn bimetallic catalysts, which is in contrast with the non-oxidative methane coupling to ethylene and aromatics. In our non-oxidative **methane conversion** study,[7] switching from Pt-Sn/SiO_2 to Pt-Sn/H-ZSM-5 (SiO_2:Al_2O_3 = 280) resulted in a 20 fold increase in the activity. STEM studies of the zeolite and silica supported catalysts and microkinetic model predictions attributed higher activity to the smaller

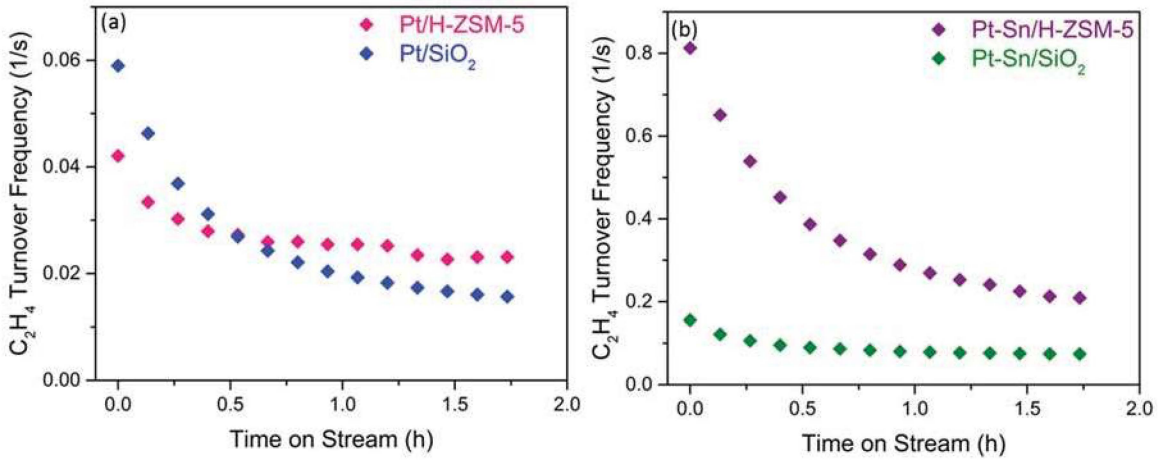

Figure 5: C_2H_4 turnover frequencies of SiO_2 and H-ZSM-5 supported catalysts. (a) Pt/SiO_2 and Pt/H-ZSM-5 (b) $Pt\text{-}Sn/SiO_2$ and Pt-Sn/H-ZSM-5. Reaction conditions of atmospheric pressure, 873 K, 12.5 Torr ethane pressure, and 0 Torr hydrogen pressure.

nanoparticles on the zeolite-supported catalyst. To analyze the **ethane dehydrogenation** reaction in this respect, Pt and Pt-Sn catalysts supported on H-ZSM-5 (SiO_2:Al_2O_3 = 280) were prepared and studied at 873 K, atmospheric pressure and with pure ethane feed. As shown in **Figure 5(a)**, the activities of the two Pt catalysts were similar over the reaction time on stream. In the case of the Pt-Sn catalysts shown in **Figure 5(b)**, the C_2H_4 TOF of the zeolite-supported catalyst with the smaller particle size was 5 times higher than that of silica supported catalyst during the initial time on stream period. However, at the end of this 2 hr experiment, this ratio decreased to approximately 2. These experimental observations agreed with our modeling predictions that, ethane dehydrogenation on PtSn catalysts is not a particularly structure sensitive reaction.

C. Pt Alloys Search and Discovery of PtZn Catalyst

We developed descriptor-based methods to efficiently screen through potential catalysts for ethane dehydrogenation**.** Based on our previous detailed understanding of this reaction through the development of PED, microkinetic models, and kinetic experiments, we concluded that the competition between C_2H_4 desorption and its dehydrogenation to vinyl is key to determining the propensity for deep C_2H_6 dehydrogenation and the undesirable coke formation. Therefore, we proposed a descriptor model for identifying promising catalysts that minimize deep C_2H_6 dehydrogenation, as shown in **Figure 6**. In particular, **Figure 6** shows the calculated Gibbs Free energy difference between the C_2H_4 desorption energy and C_2H_4's dehydrogenation barrier on the Pt-containing surfaces studied, plotted against the Gibbs Free energy barrier for the first dehydrogenation step of C_2H_6, a step which most likely determines the overall activity of a catalyst. When the Pt-containing surfaces are compared to each other for their propensity to activate C_2H_6 and their selectivity towards desorbing C_2H_4 into the gas phase over its dehydrogenation under typical experimental reaction conditions, the step site of PtZn alloy is found to be the most promising

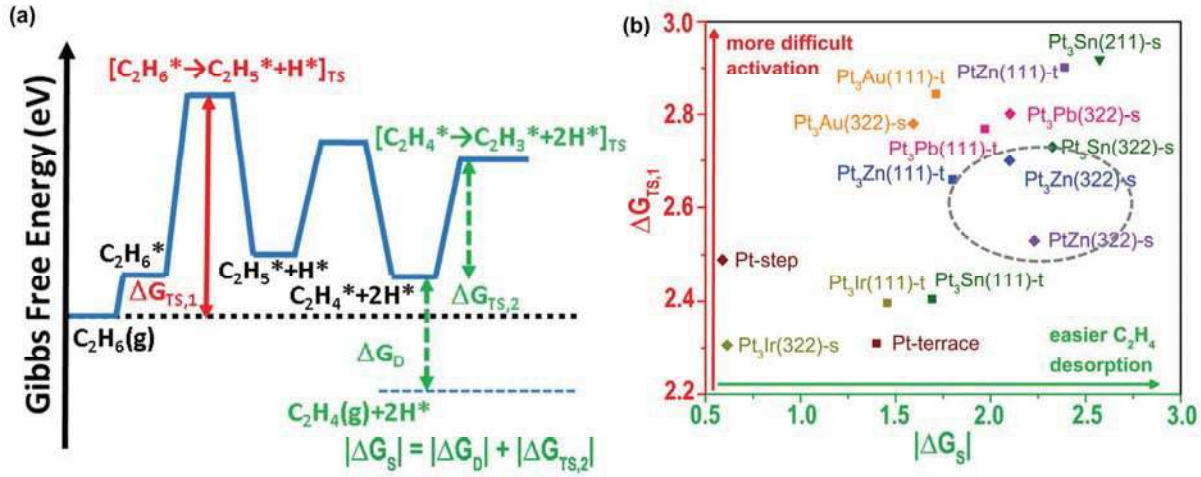

Figure 6: (a) Definition of Gibbs Free Energy values used in developing the descriptor, $\Delta G_{TS,1}$ is the Gibbs Free Energy barrier for the first dehydrogenation step of C_2H_6, ΔG_D is the Gibbs Free Energy for C_2H_4 desorption, $\Delta G_{TS,2}$ is the Gibbs Free Energy barrier for C_2H_4 dehydrogenation and ΔG_S is the sum of the absolute value of ΔG_D and the absolute value of $\Delta G_{TS,2}$ representing the selectivity of the catalyst towards desorption of C_2H_4. **(b)** Descriptor for comparing activity of Pt-containing model surfaces based on C_2H_6 first-dehydrogenation barrier (vertical axis, marked in red) and selectivity based on energy difference between C_2H_4 desorption and its dehydrogenation transition state (horizontal axis, marked in green), all in terms of Gibbs Free Energies calculated at typical reaction conditions (T = 873 K), as defined in (a). 't' denotes terrace sites; 's' denotes step sites. Gray dashed circle highlights the promising model surfaces identified through our studies.

candidate for decreasing coke precursors formation while maintaining dehydrogenation activity (Figure 6). In addition to the potential kinetic benefits of using Zn, using Zn as the promoter instead of Sn also presents financial benefits.

The potential energy diagram (PED) for ethane (C_2H_6) dehydrogenation on *step* sites is plotted in **Figure 7** for Pt(433) step, $Pt_3Sn(322)$, $Pt_3Zn(322)$, and PtZn(322). In comparison to the PED for the Pt step, both step sites for $Pt_3Zn(322)$ and PtZn(322) are shifted upward in energy, indicating that further dehydrogenation of ethylene becomes less favorable, which is desired. For $Pt_3Zn(322)$, the desorption of ethylene has a barrier of 1.21 eV, which is smaller than the barrier of further dehydrogenation of 1.43 eV. To identify the effect of Zn-rich surface composition on the ethane (C_2H_6) dehydrogenation energetics, we studied the complete reaction network and the elementary steps on PtZn(322) step surfaces in addition to the

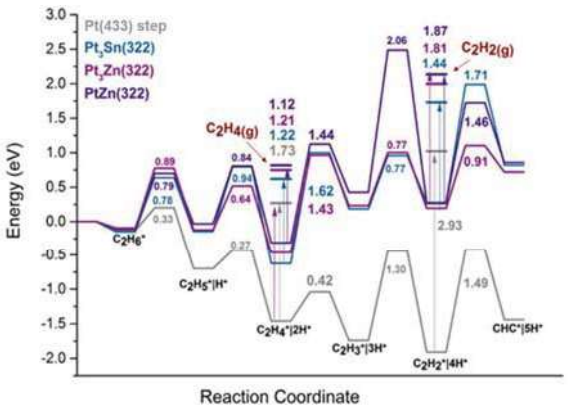

Figure 7: Calculated ethane dehydrogenation potential energy diagram (PED) based on total energies at 0 K on steps sites: Pt(433) step, $Pt_3Sn(322)$, $Pt_3Zn(322)$, and PtZn(322).

$Pt_3Zn(322)$ step. Similar to $Pt_3Zn(322)$, the respective PED for PtZn(322) is shifted even higher in energy compared to the Pt step site. On PtZn(322), the C_2H_4 desorption barrier is 1.12 eV, much smaller than the barrier for further dehydrogenation of C_2H_4 (2.06 eV). In addition, dehydrogenation from $C_2H_3^* \rightarrow C_2H_2^* + H^*$ is very disfavored for PtZn(322) with a barrier of 2.06 eV. This behavior is unlike the case for $Pt_3Zn(322)$, which has a barrier of 0.77 eV to form acetylene. Therefore, deep dehydrogenation at step sites should be suppressed by alloying Pt with Zn, and this is especially the case for Zn-rich compositions of the Pt-Zn alloys.

We also performed experiments to study the effect of bimetallic composition on the catalytic activity. Monometallic Pt and two bimetallic Pt-Zn catalysts with atomic ratios of 3:1 and 1:1, all supported on Vulcan carbon support were studied for ethane (C_2H_6) dehydrogenation at 873 K. Ethylene TOF values, defined as amount of ethylene formed per unit time normalized by the surface Pt density, are plotted with respect to the reaction time on stream in **Figure 8(a)**. We observe that, in agreement with the predictions of the DFT calculations, addition of Zn to the Pt enhanced catalytic activity. Both the initial and steady-state activities of the catalyst increased up to 2.5 times, compared to Pt/Vulcan. Pt-Zn(3:1)/Vulcan and Pt-Zn(1:1)/Vulcan compositions yield almost identical activity. A set of reaction kinetics experiments with Pt-Zn(3:1)/Vulcan showed that the apparent activation energy is 44 kJ/mol.

Based on the increase in the activity of Pt-Sn catalysts supported on H-ZSM-5 with (SiO_2:Al_2O_3 = 280) for both ethane dehydrogenation and non-oxidative methane conversion,[7-8] we repeated a similar study for the Pt-Zn system. A Pt-Zn catalyst supported on H-ZSM-5 support (SiO_2:Al_2O_3 = 280) with Pt-Zn ratio of 1:2 was prepared and studied for ethane dehydrogenation at 873 K. As shown in **Figure 8(b)**, the bimetallic catalyst supported on the zeolite yielded 25 times higher activity at the end of 2 hrs compared to the monometallic catalyst supported on the same zeolite. This finding agrees well with our DFT results,

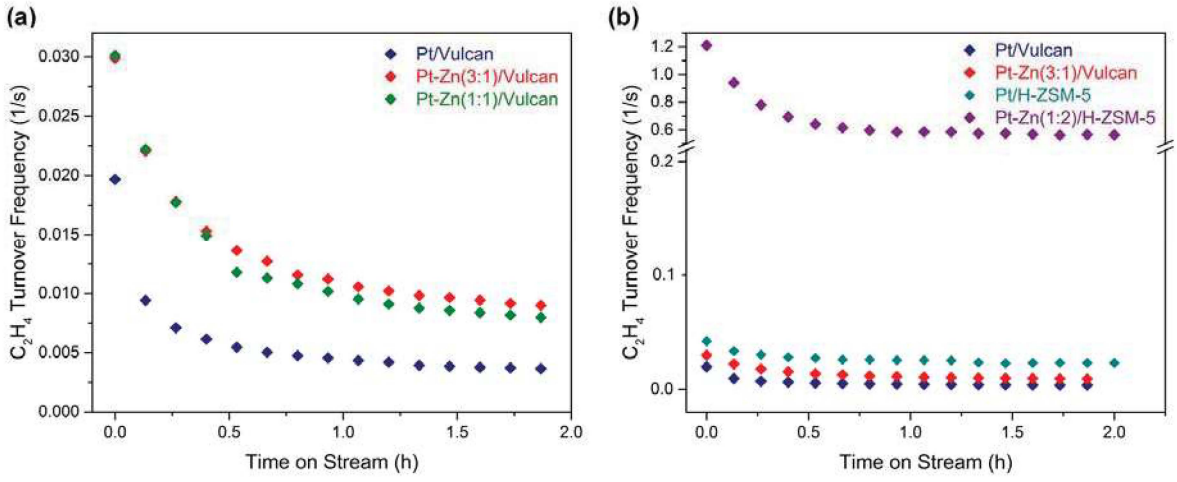

Figure 8: Ethylene (C_2H_4) turnover frequencies of (a) Pt and Pt-Zn catalysts supported on Vulcan, and (b) Pt and PtZn catalysts supported on Vulcan versus those supported on H-ZSM-5.

which suggested that deep dehydrogenation and coke deposition reactions are less likely to take place on the stepped surfaces, which are in higher percentage on smaller bimetallic particles.

D. Non-Oxidative Methane Coupling to Ethylene on PtSn Catalysts

Since ethane dehydrogenation has been observed to produce methane in the presence of co-fed hydrogen with selectivities up to 20%, we decided to study the microscopic reverse of this reaction, namely non-oxidative methane coupling to C_2H_x on Pt and PtSn catalysts supported on silica and low acidity H-ZSM-5 zeolite (Si:Al=280). As shown in **Figure 9(a),** for methane conversion on the silica supported catalysts, addition of Sn increased ethylene turnover frequency by a factor of 3 compared to pure Pt/SiO_2 catalysts. Pretreatment of the catalysts in hydrogen at 1123 K was performed to decrease the surface concentration of silanol groups on the silica surface, which decreased the extent of coke formation. Using the zeolite support further improved ethylene formation rates and selectivity towards non-coke products for the PtSn catalyst at 973 K. Subsequently, more acidic H-ZSM-5 supports were studied, whereby high formation rates for benzene and naphthalene were measured. These catalysts operated through a bifunctional mechanism. The most active and stable PtSn/H-ZSM-5 catalyst for ethylene production shown in **Figure 9(b)** (labeled as PtSn(1:3)/Z-280) formed carbon products at a rate comparable to that of state-of-the-art Mo/H-ZSM-5 catalysts for non-oxidative methane coupling.[9-12] STEM measurements identified the presence of smaller Pt nanoparticles on the H-ZSM-5 support, which might be responsible for the observed higher activity to non-oxidative methane coupling.

A microkinetic model of methane conversion was developed to gain insight into catalyst reactivity by using DFT-derived parameters for terrace and stepped surfaces of Pt and Pt_3Sn. The variations of the surface coverage of intermediates and ethylene TOF values on the Pt(433) terrace, Pt(433) step,

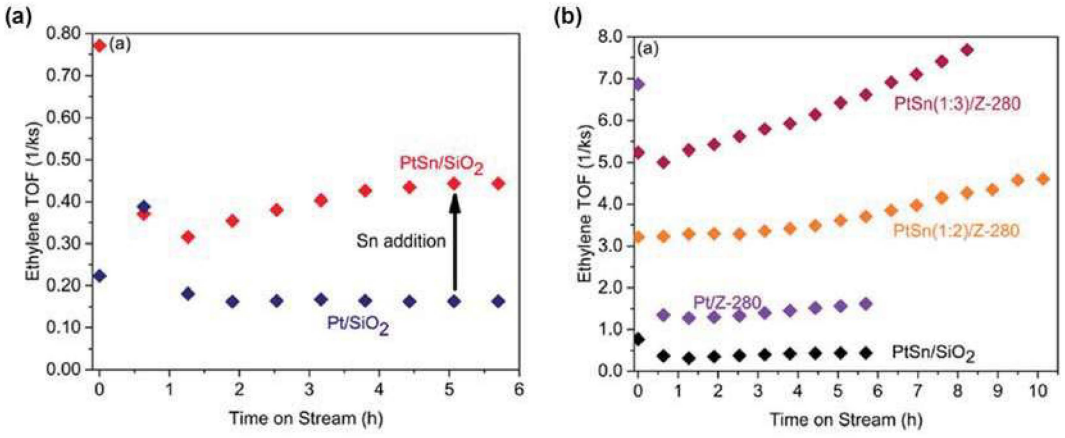

Figure 9. Ethylene TOF vs time on stream for the non-oxidative methane conversion: (a) Effect of Sn addition to Pt/SiO_2 and (b) Effect of Sn addition to Pt/Z-280 in comparison to $PtSn/SiO_2$. Conditions: 100% CH_4, flow rate 42 cm^3(STP)/min, T = 973 K, catalyst mass 1 g, P = 3 psi.

$Pt_3Sn(111)$ terrace, and the $Pt_3Sn(211)$ step surfaces are shown in **Figure 10**. Without any adjustments in the DFT-derived parameters, the model was used to predict product formation rates and variations in surface coverages of reaction intermediates under reaction conditions. The effect of Sn addition to Pt, H_2 cofeeding with CH_4, and particle size on the catalyst activity were studied by comparing model predictions with experimental results. The model predicted that terrace and steps of Pt were almost fully covered with adsorbed CH* and C* fragments, with a slightly lower total coverage on Pt step sites, corresponding to a 2.4 times higher ethylene TOF. The elementary C–C coupling step with the highest rate was found to be CH* + CH* → CHCH*, which carried 34% of the reaction flux on Pt terrace sites and 46% of the reaction flux on Pt step sites. On Pt terrace sites, the elementary step with the highest degree of rate control was the activation of methane and desorption of hydrogen, whereas on Pt steps, desorption of ethylene from the surface also had significant degree of rate control. Surface coverages of adsorbed CH* and C* were significantly lower on the $Pt_3Sn(111)$ terrace than on the Pt(111) terrace. More specifically, on $Pt_3Sn(111)$ terrace, the coverage of adsorbed CH* decreased to 0.28 from 0.92 on the Pt(111) terrace. Furthermore, 50% of the sites on the $Pt_3Sn(111)$ terrace were calculated to be vacant while Pt(111) terrace was found to be mostly covered by reaction intermediates. The elementary C–C coupling step with the highest rate on the $Pt_3Sn(111)$ terrace was identified to be CH_2* + C* → CH_2C*, which carried 49% of the reaction flux, and similarly to the Pt terrace, methane activation possessed the highest degree of rate control for ethylene formation.

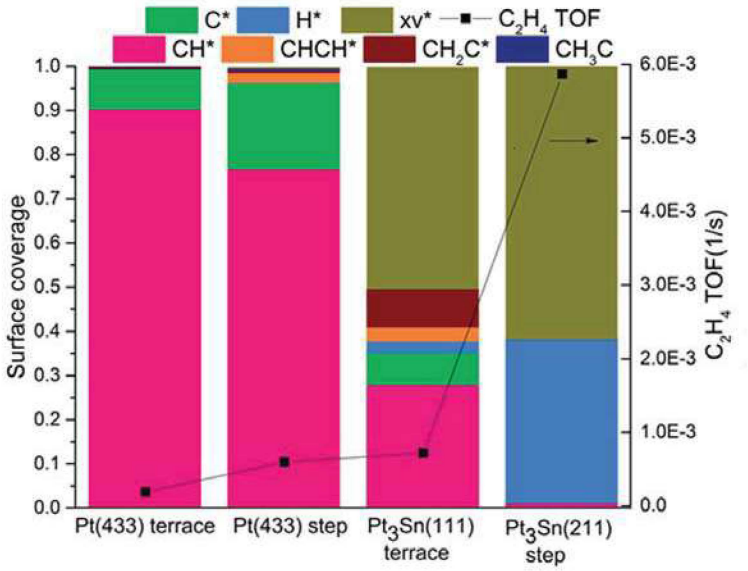

Figure 10. Surface coverages and ethylene TOF values of the studied surfaces predicted by the microkinetic model for no H_2 cofeeding conditions. The left axis shows surface coverages of the indicated species, and the right axis shows the ethylene TOF values. Conditions: 100% CH_4, flow rate 42 cm^3(STP)/min, T = 973 K, catalyst mass 1 g, P = 3 psi.

We also analyzed the reactivity of methane on the terrace and stepped $Pt_3Sn(211)$ surfaces. The microkinetic model predicted that the stepped $Pt_3Sn(111)$ surface was cleaner than Pt(111), with 62% of its sites vacant, under typical reaction conditions. The predominant elementary C–C coupling step was CH* + CH* → CHCH*. Similarly to the other surfaces, activation of methane was the rate-controlling step. The Pt_3Sn step possessed the highest predicted activity with a TOF 9.9 times higher than Pt(433)

step. We also predict that Pt_3Sn step sites are more active than Pt_3Sn terrace sites. Based on this microkinetic model, we would expect that these PtSn alloys are more active for smaller sized nanoparticles where there is a higher fraction of step sites. This prediction is in agreement with the STEM measurements and experimental kinetic data, which identified the presence of smaller Pt nanoparticles on the H-ZSM-5 support; these smaller nanoparticles might be responsible for the observed higher activity of the H-ZSM-5-supported PtSn catalysts for non-oxidative methane coupling.

University of Wisconsin Publications

1. Gerceker, D.; Dumesic, J. A.; Mavrikakis, M., Ethane Dehydrogenation on Pt-Zn surfaces: Effect of composition. *To be submitted.*
2. Gerceker, D.; Hussan, A.; Dumesic J. A.; Mavrikakis, M., Ethane Dehydrogenation over Pt and Pt-Sn Catalysts: A Combined Experimental and Computational Study. *To be submitted.*
3. Peng, G.; Gerceker, D.; Kumbhalkar, M.; Dumesic, J. A.; Mavrikakis, M., Ethane dehydrogenation on pristine and AlO_x decorated Pt stepped surfaces. *Catalysis Science & Technology* **2018,** *8* (8), 2159-2174.
4. Tacey, S. A.; Xu, L.; Szilvási, T.; Schauer, J. J.; Mavrikakis, M., Quantum chemical calculations to determine partitioning coefficients for $HgCl_2$ on iron-oxide aerosols. *Science of The Total Environment* **2018,** *636*, 580-587.
5. Chen, C.; Tao, Z.; Carr, A.; Matyba, P.; Szilvási, T.; Emmerich, S.; Piecuch, M.; Keller, M.; Zusin, D.; Eich, S., Distinguishing attosecond electron–electron scattering and screening in transition metals. *Proceedings of the National Academy of Sciences* **2017,** *114* (27), E5300-E5307.
6. Merte, L. R.; Bai, Y.; Zeuthen, H.; Peng, G.; Lammich, L.; Besenbacher, F.; Mavrikakis, M.; Wendt, S., Identification of O-rich structures on platinum (111)-supported ultrathin iron oxide films. *Surface Science* **2016,** *652*, 261-268.
7. Tao, Z.; Chen, C.; Szilvási, T.; Keller, M.; Mavrikakis, M.; Kapteyn, H.; Murnane, M., Direct time-domain observation of attosecond final-state lifetimes in photoemission from solids. *Science* **2016,** *353* (6294), 62-67.
8. Yeh, Y.-H.; Gorte, R. J.; Rangarajan, S.; Mavrikakis, M., Adsorption of small alkanes on ZSM-5 zeolites: influence of Brønsted sites. *The Journal of Physical Chemistry C* **2016,** *120* (22), 12132-12138.
9. Zhang, Y.; Yu, J.; Yeh, Y.-H.; Gorte, R. J.; Rangarajan, S.; Mavrikakis, M., An adsorption study of CH4 on ZSM-5, MOR, and ZSM-12 zeolites. *The Journal of Physical Chemistry C* **2015,** *119* (52), 28970-28978.

10. Kudernatsch, W.; Peng, G.; Zeuthen, H.; Bai, Y.; Merte, L. R.; Lammich, L.; Besenbacher, F.; Mavrikakis, M.; Wendt, S., Direct visualization of catalytically active sites at the FeO–Pt (111) interface. *ACS nano* **2015,** *9* (8), 7804-7814.
11. Matyba, P.; Carr, A.; Chen, C.; Miller, D. L.; Peng, G.; Mathias, S.; Mavrikakis, M.; Dessau, D. S.; Keller, M. W.; Kapteyn, H. C., Controlling the electronic structure of graphene using surface-adsorbate interactions. *Physical Review B* **2015,** *92* (4), 041407.
12. Cattelan, M.; Peng, G.; Cavaliere, E.; Artiglia, L.; Barinov, A.; Roling, L. T.; Favaro, M.; Píš, I.; Nappini, S.; Magnano, E., The nature of the Fe–graphene interface at the nanometer level. *Nanoscale* **2015,** *7* (6), 2450-2460.
13. Peng, G.; Mavrikakis, M., Adsorbate diffusion on transition metal nanoparticles. *Nano letters* **2014,** *15* (1), 629-634.
14. Merte, L. R.; Bechstein, R.; Peng, G.; Rieboldt, F.; Farberow, C. A.; Zeuthen, H.; Knudsen, J.; Lægsgaard, E.; Wendt, S.; Mavrikakis, M., Water clustering on nanostructured iron oxide films. *Nature communications* **2014,** *5*, 4193.

University of Wisconsin students and postdocs partially supported by the project

Duygu Gerceker (PhD student)
Jake Gold (PhD student)
Guowen Peng (Postdoc)
Srinivas Rangarajan (Potsdoc)
Sean Tacey (PhD student)

II. Sub-nano cluster catalyst work

Scott L. Anderson, Chemistry Dept. University of Utah
Anastassia N. Alexandrova, Chemistry and Biochemistry, University of California, Los Angeles

This part of the effort focused on use of Pt and Pt alloys in the form of sub-nano clusters, where essentially all the Pt atoms are available as catalytic sites. The fact that Pt atoms in clusters are under-coordinated, or coordinated with many non-Pt atoms, results in properties that depend on both cluster size and the type of dopant/alloying atoms, and also on the metal-support interaction. These special features of sub-nano clusters provide additional tools for optimizing activity and selectivity, but it can be challenging to understand and use the size-dependent properties to optimize catalyst activity and selectivity, and to stabilize the clusters against processes such as Ostwald ripening or diffusion and agglomeration that increase the cluster size, thus reducing the available catalytic surface area.

In the course of this grant, Alexandrova developed a new paradigm for theoretical modeling of cluster catalysis, which describes these systems as ensembles of many structural forms thermally populated in conditions of catalysis, and easily interconverting, thermally and under the influence of changing adsorbates in the reaction. This paradigm required new theoretical methods. The development was possible through a tight collaboration with Anderson, who provided detailed experimental data and tested some of the predictions. The statistical ensemble catalyst description, though complex, enabled testable predictions and interpretations of observed size-activity dependences for cluster catalysts, and the effects of dopants on stability and catalytic selectivity. These developments also led to findings of fundamentally different properties that such dynamic catalytic interfaces can have, in contrast to more stationary extended surfaces.

Anderson developed new tools for preparing and characterizing sub-nano *alloy* cluster catalysts, with control over size and composition. The new approach allows study over a much wider range of cluster sizes than could previously be studied.

A. Cluster size effects on activity

As a baseline, consider the temperature-programed desorption/reaction (TPD/R) data for ethylene (C_2D_4) adsorption, desorption, and dehydrogenation on small Pt_n clusters supported on an alumina film grown on Ta(110).[13] Here, the goal is to have ethylene desorb intact from the catalyst surface, rather than undergoing deep dehydrogenation that results in carbon deposition on the surface. The red trace in Fig. 11 shows the results for the alumina support with no Pt clusters – only intact C_2D_4 is observed, desorbing at low temperatures corresponding to desorption energy of ~0.5 eV. For the Pt_n/alumina samples, the first TPD/R run (black trace) shows low temperature ethylene desorption from the alumina support, together with a broad feature peaking near 300 K ($E_{desorption}$ = ~0.7 to 1.2 eV) that clearly corresponds to ethylene binding to Pt_n. Just below 300 K, D_2 desorption is observed,

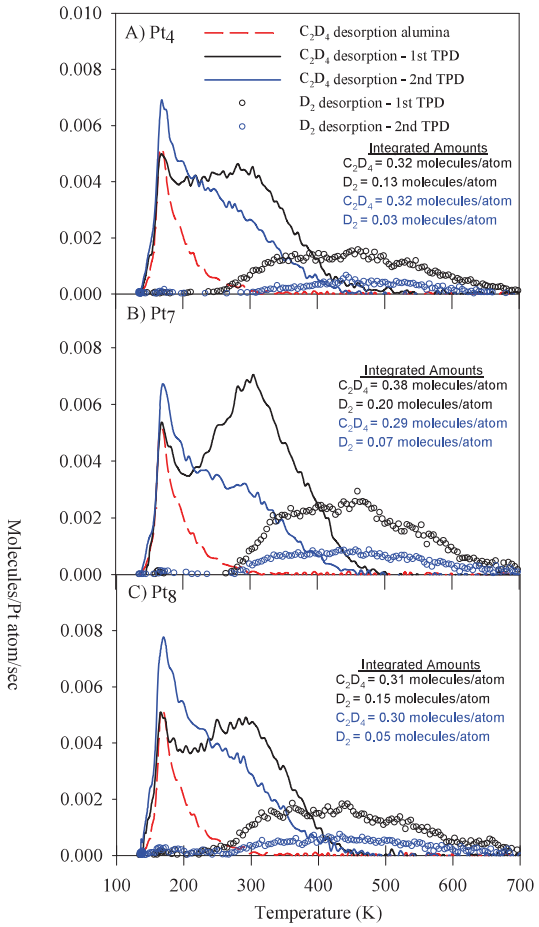

Fig. 11. Desorption of C_2D_4 and D_2 from Pt_n/alumina.

indicating the onset of dehydrogenation. At that point, intact ethylene quickly stops desorbing, and since no C_2H_2 or other carbon-containing products are observed to desorb, the implication is that, as soon as ethylene begins to dehydrogenate, only hydrogen desorbs, depositing carbon.

The figure gives the number of C_2D_4 and D_2 molecules desorbing *per* Pt atom, and the total number of C_2D_4 molecules adsorbed initially can be estimated as C_2D_4 +0.5 D_2. Note that Pt_7 gives substantially more C_2D_4 and D_2 desorption, i.e., it provides more ethylene binding sites *per* atom than either Pt_4 or Pt_8. This is an example of one type of cluster size effect – that some clusters provide additional sites or sites with different binding energy or chemistry, compared to other sizes.

The effect of heating/carbon deposition can been seen if the sample is cooled and exposed to additional C_2D_4, for a 2nd TPD/R run (blue traces): 1. Less C_2D_4 adsorbs initially (fewer binding sites) and its desorption shifts to lower temperatures (weaker binding). 2. Correspondingly less D_2 desorption is observed. Examination of the surface by XPS and ISS shows deposition of carbon, and loss of Pt from the top-most sample layer, all showing that the catalyst was rapidly deactivated by a combination of coking and sintering.

Theory provides clear explanations for all these observations. For example, it is found that all the Pt_n have several thermally accessible structures, even at room temperature, but that Pt_7 accesses more of them, and a significant fraction of structures are single layer with all Pt atoms exposed in the surface, whereas Pt_8 has a stable prismatic 3D global minimum that does not easily isomerize, and where not all the Pt is on the surface. In addition, ethylene adsorption drives isomerization to accommodate even more molecules, as shown for Pt_7 in Fig. 12. On the right side, the prismatic, global minimum structure is shown with 1, 2, and 3, ethylene adsorbed (Note: only the lowest energy structures are shown – many additional isomers were characterized[13]). The left-most image shows the lowest energy single-layer Pt_7 isomer with one adsorbed ethylene. For adsorbate-free Pt_7, this single-layer isomer is only ~0.2 eV above the prismatic global minimum, but note that the ethylene adsorption energy ($E_{1ethylene}$) is 0.7 eV higher on the single layer isomer, i.e., it becomes the global minimum for ethylene-Pt_7. By the time 3 ethylene are adsorbed, the prismatic isomer spontaneously isomerizes to a single layer structure. Additionally, this stronger binding to single-layer isomers favors the di-σ binding mode, which is a known precursor for dehydrogenation, suggesting that Pt_7 should have a higher propensity for dehydrogenation, in

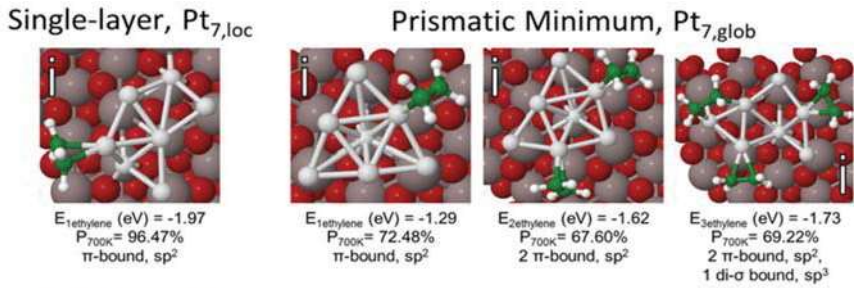

Fig. 12. Structures and energetics of single layer and prismatic Pt_7 with ethylene

agreement with experiment. Being able to model this kind of thermal and adsorption-driven dynamical behavior is crucial to understanding the chemistry and stability of sub-nano clusters.

B. Alloying/doping strategies for controlling dehydrogenation and anti-coking properties

Theory in Alexandrova group led the way in predicting new dopants or alloying elements that could enhance the selectivity of catalytic dehydrogenation. First, inspired by the work on bulk catalytic surfaces of Co and Ni, boron was proposed as a possible dopant for Pt clusters[14] Jointly with Anderson, the effects of boration of supported, size-selected Pt clusters on alumina was tested and confirmed.

First, however, it was necessary to develop a new approach to making size- and composition-selected sub-nano alloy cluster catalysts. Anderson had previously developed, with AFOSR support, a mass-selected cluster source that can be used to deposit size-selected metal clusters with sufficient coverage to allow catalysis studies. The difficulty is that for many bimetallic combinations, the elements involved have multiple stable isotopes, so that for clusters of more than a few atoms, it becomes impossible to cleanly select a particular size and stoichiometry. For example, the isotope distribution in Pt is 6 amu wide, and boron has both ^{10}B and ^{11}B isotopes. Therefore, for clusters containing more than a few Pt atoms, the mass distributions for Pt_nB_m, $Pt_nB_{\pm1}$ overlap, so that one composition cannot be selected cleanly by mass. The same is true for many bimetallic combinations, for example, the Pt_nSn_m clusters discussed below. There, both metals have broad isotope distributions, and for clusters of more than ~ten atoms in total, every single mass number has contributions from 2 to 4 different clusters with very different Pt:Sn ratios.

Therefore, a new strategy was developed to make size- and composition selected clusters. The idea was to deposit size-selected seed clusters on the surface (e.g. Pt_n), then to use a *self-limiting* reaction to selectively deposit a controlled amount of the second element on the seed clusters. In this approach, it is critical that the reaction be self-limiting, and that it not happen non-specifically on the catalyst support, otherwise only the average stoichiometry can be controlled.

For the case of adding boron, the process was simple. Samples containing size-selected Pt_n seed clusters were simply exposed to diborane at low temperatures, then gently heated to decompose the diborane. Experimentally it was found that boron deposited ~10 times more efficiently on the Pt clusters than on the aluminum support, and furthermore, that the small amount of boron bound to the support had no effect on the catalysis by the supported PtB clusters. The resulting Pt:B stoichiometry was close to 1:1, independent of the diborane dose on the samples, i.e., the reaction is self-limiting, presumably controlled by how many diborane molecules can bind to a Pt_n cluster. DFT showed that after mild heating to drive off the hydrogen, the boron atoms migrated underneath the Pt clusters, forming Pt-B-O bonds that anchor the clusters to the support.

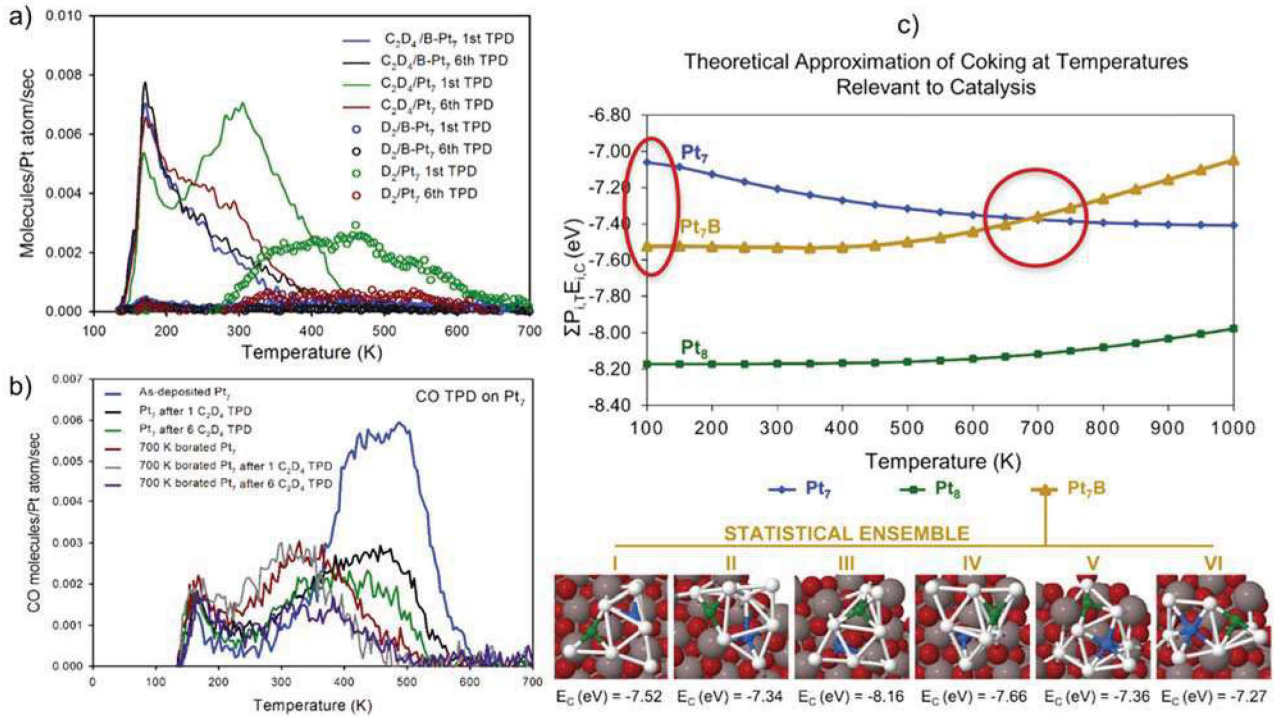

Fig. 13. Coking resistance of borated Pt clusters form experiment and theory: (a,b) experimental TPD of ethylene of CO, demonstrating that after several cycles of ethylene dehydrogenation the Pt sites are still all accessible; (c) theory predicts that borated clusters become more and more coke-resistance at rising T, due to enrichment of the ensemble with species of smaller coke affinity, in agreement with experiment.

The effects on dehydrogenation chemistry are summarized in Fig. 13. The upper left frame compares the ethylene and D_2 desorption from Pt_7/alumina and Pt_7B_6/alumina. As shown in Fig. 11, for Pt_7, the first TPD/R run gave a large ethylene desorption component around 300 K, but also considerable D_2 desorption, indicating deep dehydrogenation to deposit carbon. The 2nd TPD/R run showed diminished ethylene binding and D_2 desorption because the catalyst was coked up in the first run. For borated Pt_7, note that the ethylene desorbed at much lower temperatures, such that it had mostly desorbed prior to the onset temperature for dehydrogenation. As a result, much less D_2 was observed, showing that not much carbon deposition occurred. Because coking was suppressed, the TPD/R behavior was stable from run to run. The lower left frame of the figure shows CO TPD experiments, used to probe the number and energetics of exposed Pt binding sites. Results are shown for the as-prepared Pt_7 and borated Pt_7 clusters, and for the clusters after either one or six sequential cycles of ethylene adsorption, desorption, and dehydrogenation. Note that even a single ethylene TPD/R run caused a dramatic decrease in the availability of Pt sites for CO, and that the site availability continued to decrease after six ethylene TPD/R runs. In contrast, for borated Pt_7, one ethylene TPD/R run had essentially no effect on the Pt site availability, although there still was site loss after 6 TPD/R runs.

The right top frame of Fig. 13 shows a theoretical estimate of the coking resistance for Pt_7, Pt_7B, and Pt_8 as a function of temperature, based on the distribution of cluster isomers calculated to be present. At high temperatures, coke-resistant isomers predominate for Pt_7B, compared to the pure Pt clusters. The bottom right frame shows examples of the structures calculated for Pt_7B with one carbon atom added.

C. Pt-Sn clusters

To selectively produce Pt-Sn alloy clusters, a somewhat more complex reaction process was used, compared to that used for boron. The idea is similar to the kind of two-step chemistry used in atomic layer deposition. First size-selected Pt_n were deposited on either silica or alumina supports, then exposed to H_2, which efficiently dissociates on Pt_n, but not the oxide supports. Next $SnCl_4$ was dosed, reacting with the H-covered Pt clusters, liberating HCl, and leaving Sn, along with some Cl, bound to the clusters. To remove more Cl, the samples were dosed with H_2 again, with additional HCl observed to desorb. At that point clusters had less than 10% of the original Cl present, and by simply heating the clusters to 700 K, the rest of the Cl desorbed as HCl, along with residual H_2. X-ray photoelectron spectroscopy (XPS) showed that the Sn deposition process was quite selective – depositing Sn about 50 times more efficiently on Pt sites, compared to sites on the alumina or silica supports. The stoichiometry revealed by XPS ranged from near 1:1 for small clusters (e.g. $Pt_4Sn_{3.3}$, $Pt_7Sn_{6.3}$) to more like 3:1 for large clusters (e.g. $Pt_{24}Sn_{7.6}$). The difference was attributed to the structure of the seed clusters – small clusters have essentially all their Pt atoms in the surface layer where they can bind H and Sn, whereas larger clusters are three dimensional, with some atoms in the interior where they are not involved in the chemistry.

Tin addition has a dramatic effect on the propensity of ethylene to undergo deep dehydrogenation leading to carbon deposition. The left side of Fig. 14 shows the 1st and 2nd ethylene TPD/R runs for Pt_4, Pt_7, and Pt_{24} deposited on a silica support (results for Pt-free silica shown in pink). As in the Pt_n/alumina presented above, during the first TPD/R run (black) there is significant ethylene desorption around 300 K, but then as dehydrogenation sets in, the remaining ethylene stops desorbing and is converted to carbon on the surface. As a result, the 2nd run on each sample (blue) showed significant changes in the amount and temperature dependence of ethylene and D_2 desorption. There is also evidence from ion scattering that sintering is relatively severe for Pt/silica, leading to loss of Pt surface area.

The right frames show analogous data for Sn-alloyed clusters. The red trace is actually for the final step in the Sn alloying process – heating to drive off residual H and Cl. For this figure, the samples were dosed with ethylene *before* heating to drive off H and Cl, and it can be seen that not as much ethylene desorbs, because the presence of H and Cl blocks ethylene adsorption on many sites. In the 2nd and 3rd TPD/R runs, it can be seen that the amount of ethylene desorbing recovers. Note also that the clusters bind ethylene with energy (i.e., desorption temperature) similar to that in the bare Pt clusters, however, there is essentially no D_2 desorption, i.e., no coking. In addition, the samples appear to be more

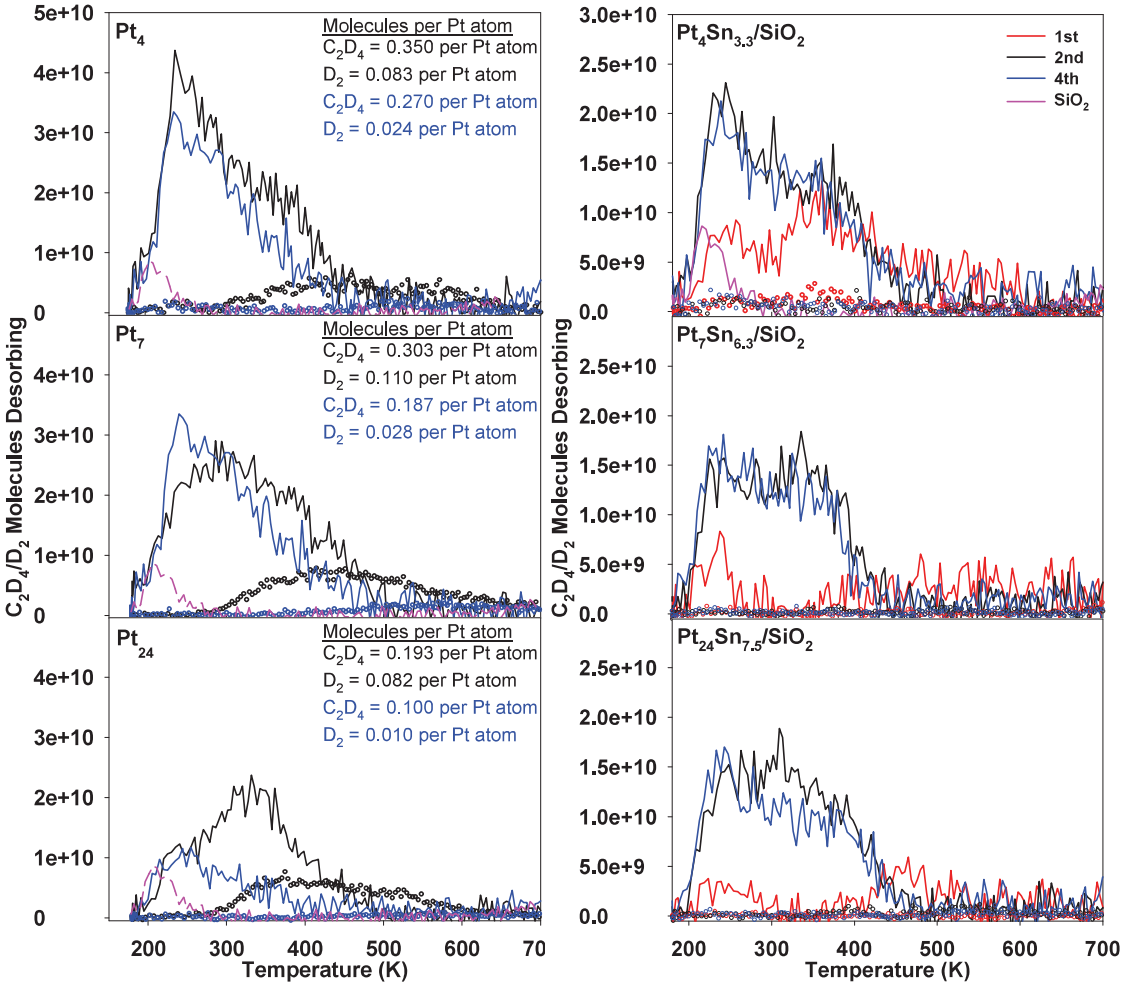

Fig. 14. Left: Ethylene TPD/R from Pt_n/silica, showing substantial deep dehydrogenation and deactivation. Right: Analogous results for Pt_nSn_x/silica, showing high stability and negligible deep dehydrogenation. Note: the 1st run in this case was for freshly prepared samples never previously heated, and therefore still having significant H and Cl on the surface. Note the large change from the 1st to 2nd run, but no subsequent changes.

thermally stable than Sn-free Pt clusters on silica. Similar effects were observed for tin alloying of Pt_n on alumina supports.

DFT-based global optimization was performed for PtSn clusters on a model amorphous silica support, focusing on Pt_4Sn_3 as a computationally tractable system. In Pt_4Sn_3 clusters without adsorbed ethylene, thorough mixing of Pt and Sn was observed, i.e., these are alloy clusters, rather than Pt clusters decorated with Sn. A great variety of structural forms was found, all with fully quenched spin, due to the presence of covalent PtSn bonds. The clusters have very few opportunities for the di-σ ethylene binding that tends to promote deep dehydrogenation, because most of Pt atoms are separated by Sn. In all cases, ethylene preferentially binds to the clusters in the π mode, because of the lack of unpaired spins (Fig. 15). Ethylene is not activated toward dehydrogenation, in agreement with experiment. Analogous results were obtained for alumina-deposited PtSn.

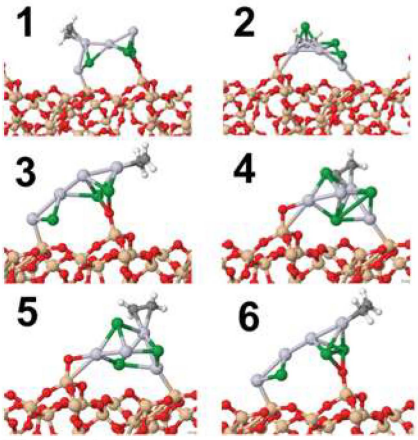

Isomer	E(eV)	2S+1	$Q_{cluster}$(e)	Mode	C-C(A)
1	0	1	-0.03	pi	1.41
2	0.001	1	-0.03	pi	1.41
3	0.170	1	-0.04	pi	1.40
4	0.171	1	-0.04	pi	1.40
5	0.265	1	0.08	pi	1.43
6	0.313	1	-0.13	pi	1.41
7	0.314	1	-0.12	pi	1.41
8	0.365	1	-0.12	pi	1.41
9	0.442	1	-0.10	pi	1.41
10	0.484	1	-0.10	pi	1.41

Figure 15. Lowest energy isomers of Pt_4Sn_3 deposited on amorphous silica: (LEFT) structures predicted by global optimization at a DFT level; (RIGHT) Table listing the energy difference from the global minimum, total spin (all clusters are singlets), amount of electron transfer from the support, the mode of ethylene binding (always π, and never di-σ), and the length of the C-C bond in ethylene.

A paper on the method used to prepare size- and composition-selected Pt_nSn_m clusters is under revision for J. Phys. Chem. C. Two additional papers are in preparation, one authored by each of the lead students in theory and experiment. One will discuss the effects of Sn alloying on the structure of the clusters and their thermal stability. The other will discuss the effects on ethylene desorption and dehydrogenation and the coking stability of the clusters. We also have a complete set of reactivity data for PtSn clusters on alumina supports, and most of the DFT work is also complete. Pending completion of a few more physical characterization experiments, an additional paper will be written describing those results.

D. Survey calculations suggest new and better dopants for coke control.

Si and Ge were identified as promising new dopants for Pt, which we so far studied only theoretically. We found them via computational screening, using such parameters as stability against sintering, coke resistance, and inability of ethylene activation while being able to dehydrogenate ethane. All the dopants identified to date (B, Sn, Si, Ge) are inexpensive metalloids, but, interestingly, their effects of the electronic structure of Pt clusters are not the same. While B mainly seems to reduce the electron transfer to the cluster from the support, binding between the cluster and support, Si, Ge, and Sn mix with and form covalent bonds with Pt. Si/Sn/Ge are therefore exposed to the cluster surface. As a result of the covalency of bonding, the open spins of Pt get quenched. This means that for the dehydrogenation to happen, a spin crossover needs to happen first, and that is an energetically costly process. In addition, not having two adjacent Pt atoms on the cluster prevent ethylene binding in the di-σ mode without cluster rearrangement.

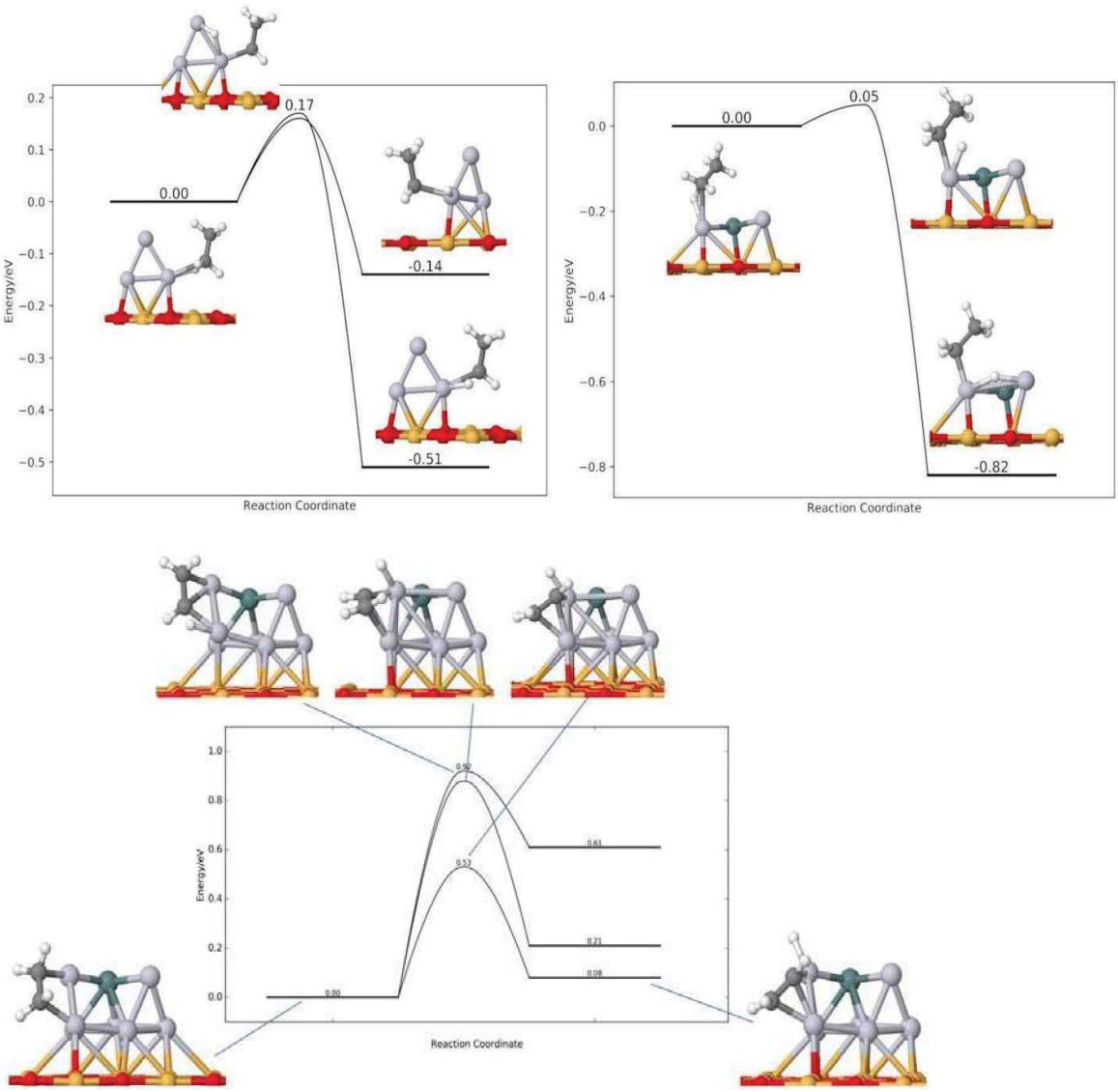

Figure 16. (TOP) Reaction pathway for direct ethane dehydrogenation on Pt_3 (left) and Pt_2Ge (right). Activation energies are given in eV. O, Mg, Pt, Ge, C and H are depicted in red, orange, grey, dark green, dark grey and white respectively. (BOTTOM) Reaction pathways for direct ethylene dehydrogenation on Pt_7Ge, Isomer I, with TSs and the final product structures shown. Activation energies are given in eV. O, Mg, Pt, Ge, C and H are depicted in red, orange, grey, dark green, dark grey, and white respectively.

Si and Ge have effects on the Pt cluster functionality similar to that of Sn, but at least in the case of Ge, the performance is predicted to be even better. Si/Ge both mixed well with Pt, and are present on the cluster surface. They separate Pt sites and remove Pt-Pt bonds, bind to Pt covalently, and quench all unpaired spins, in all low-energy PtSi/Ge isomers. As a result, di-σ binding of ethylene is energetically inaccessible. Again, a statistical ensemble of many cluster shapes was considered in every case, for more realistic representation of the system. Importantly, Ge appears to dehydrogenate ethane nearly

spontaneously, unlike PtB. At the same time, Ge-doped Pt clusters have a significant barrier toward dehydrogenation of ethylene (whereas pure Pt dehydrogenates ethylene with a very small barrier). Our predictions await experimental demonstration. It should be possible to create PtGe alloy clusters in a manner similar to that used for PtB clusters, using, for example tetramethylegermane as the deposition reactant. There are a number of different organogermane reactants available commercially, which should allow some control over the PtGe stoichiometry. PtSi alloys can be made with silane or organosilicon reactants.

E. Fundamental theory of dynamic catalytic interfaces – contrast to the usual

Our key fundamental theoretical finding is that cluster catalysts must be described by the ensemble of many energetically accessible isomers, rather than just the lowest energy structure, and that the most stable isomer is likely not the most active one. We developed methods for ensemble discovery (variants of global optimization), and also for finding the kinetically-accessible pathways for catalyst isomerization. For various minima, we first perform structure matching to find the most geometrically-related isomers. Next, we use the nudged elastic band (NEB) method to model isomerization, assisted by a force field that performs a slight adjustment of the image geometries to avoid collisions and promote convergence. Of the many pathways found, we pick the lowest-energy ones and build a connectivity tree (Fig. 17). This work informed us that sub-nano clusters can visit dozens of distinct geometric states in under 1 ns at 700 K (typical temperature for dehydrogenation). We

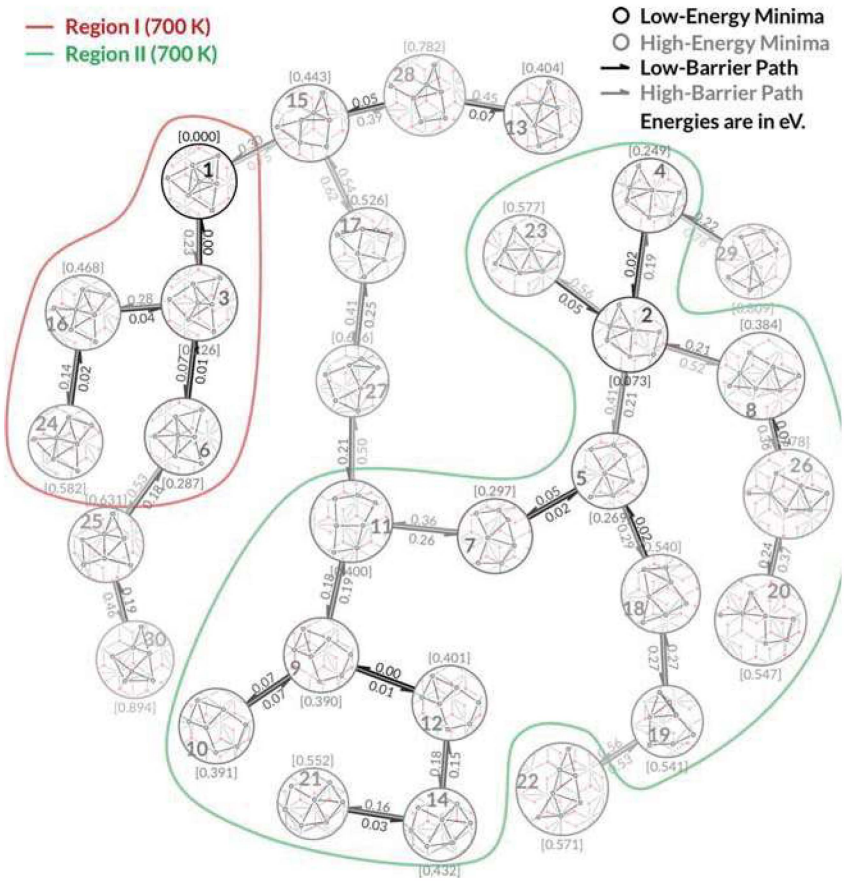

Fig. 17 Pt_7 on Al_2O_3: isomerization, connectivity tree. Barriers to isomerisation are shown. All minima can be visited by the system in under 1 ns. Regions outlines in red and green feature particularly facile isomerization.

conclude that the many cluster shapes can be expected to be generally all kinetically accessible. We note that such a study is very computationally expensive. It would be impossible to repeat it for every studied system.

Fluxionality does not mean only geometric change. It may also involve changing of the cluster-binding site on the support, as well as changing chemical composition. For example, in a study of oxidative dehydrogenation of cyclohexane on Pd and Cu oxide clusters, Vajda and Alexandrova found that both clusters undergo partial reduction at catalytically interesting temperatures. This change of oxidation state, as well as catalyst restructuring, were found to be responsible for the remarkable C6 selectivity of these catalysts: PdO produced mainly benzene, whereas CuO clusters produced cyclohexene and no benzene. Hence, cluster fluxionality should be understood more broadly than just a structural change.

There are many unusual consequences of the extreme fluxionality of the catalytic interface. The ensemble of the catalyst states restructures in every reaction intermediate. Kinetics is controlled by the most active cluster structures, which are not the most stable. Therefore, every TS and every minimum on the reaction profile is governed by a different state of the catalyst. As a result, scaling relations break down, more as a rule than as an exception. This means that it should be possible to perform catalyst optimization beyond the limit imposed by linear free energy scaling relationships. Catalytic processes are likely to exhibit non-Arrhenius behavior, etc.

F. In situ study of Pt_n/silica by X-ray techniques

X-ray scattering methods are commonly used to study catalysts, and in this project we applied grazing-incidence small angle X-ray scattering (GISAXS) and grazing-incidence X-ray absorption spectroscopy (GIXAS) to size-selected Pt_n/silica catalysts. This work was done in collaboration with the groups of Randall Winans and Sungsik Lee at Argonne National Laboratory.

We were able directly detect and characterize Pt_{24} clusters by GISAXS, but Pt_2 and Pt_{13} proved too small to give scattering significantly above the background from disorder in the silica support. Nonetheless, this results showed that Pt_{24} did not sinter or aggregate at room temperature, and that if Pt_2 or Pt_{13} sintered at all, they did not generate particles in the >20 atom range which would have been detectable. For Pt_{24}, thermal sintering was observed only for temperatures above 100 °C.

The most important result of this study relates to the common use of X-ray absorption near-edge spectroscopy (XANES) to identify the oxidation state of metals in catalysts. In XANES of Pt_n/silica, the Pt L_3 edge was observed to shift to higher energy for decreasing Pt cluster size, and a “white line” feature was observed, well above the intensity for a bulk Pt reference sample. Typically, such changes would be attributed to oxidation of the cluster from air exposure, but we also measured X-ray photoelectron spectra of the sample before and after room temperature air exposure. There was no sign that the Pt in the samples formed anything like a stoichiometric oxide, such as PtO or PtO_2 upon air exposure. Instead, we

demonstrated that there are large size-dependent final state effects for sub-nano cluster samples that give shifts similar to those seen for oxidation. This result shows that for sub-nano catalysts, increasingly of interest in the catalysis field, interpretation of XANES is not straightforward, and must consider both oxidation state and final state effects.

G. Energetic nanoparticle synthesis and characterization

Part of the Anderson group effort on the project has been in developing methods to synthesize boron and aluminum nanoparticles capped with organic layers that help stabilize and passivate the unoxidized particle surface, and to render the particles dispersible in fuels or propellants of interest. We also characterize the size, structure, and surface chemistry of the particles. During the past grant period, most of the energetic nanoparticle work was in collaboration with AFRL groups who did both physical and combustion characterization. During this project period, the following studies were completed and published.

1. "Aluminum Nanoparticle Production by Acetonitrile-Assisted Milling: The Effects of Liquid vs. Vapor Phase Milling, and of Milling Method on Particle Size and Surface Chemistry." Jiang Yu, Brandon McMahon, Jerry Boatz, and Scott Anderson, J. Phys. Chem. C 120 (2016), 19613–19629 DOI: 10.1021/acs.jpcc.6b04054. In this study we showed that *vapor* phase acetonitrile is an extremely efficient reactant for producing highly reactive Al nanoparticles by attrition from solid Al spheres in a planetary mill. Theory from Boatz at AFRL/Edwards AFB helped to understand the mechanism for the efficient reaction of acetonitrile vapor with unpassivated aluminum surfaces. This synthesis method has become our go-to method for generating large quantities of aluminum nanoparticles for testing.
2. "Borane-Aluminum Surface Interactions: Enhanced Fracturing and Generation of Boron-Aluminum Core-Shell Nanoparticles", Jiang Yu, Jerry A. Boatz, and Scott L. Anderson, J. Phys. Chem. C 121, (2017) 14176–14190, DOI: 10.1021/acs.jpcc.7b03583. In this project, we discovered that diborane and pentaborane are also efficient milling agents for Al nanoparticle production, generating highly reactive particles with borane-like surface functionality. The borane functionality can be used to bind capping agents such as alkyl groups and ionic liquid molecules. Again, theory from Boatz at AFRL/Edwards AFB was essential in understanding the chemistry responsible for the enhanced size reduction.
3. "Combustion Behavior of High Energy Density Borane-Aluminum Nanoparticles in Hypergolic Ionic Liquids", Jiang Yu, Tonya N. Jensen, William K. Lewis, Christopher E. Bunker, Steven P. Kelley, Robin D. Rogers, Owen M. Pryor, Steven D. Chambreau, Ghanshyam L. Vaghjiani, and Scott L. Anderson, Energy and Fuels, 2018, 32 (7), pp 7898–7908. DOI: 10.1021/acs.energyfuels.8b01334. In this project, borane-capped Al nanoparticles were further

capped with several hypergolic ionic liquids, and then the effects of high particle loadings on hypergolic ignition were studied at AFRL/Edwards AFB. Complementary high speed photographic ignition characterization was done by a group at McGill University and University of Alabama. The borane-capped particles were characterized by XRD and TGA/DSC by researchers at AFRL/Wright-Patterson AFB. In addition, we developed a procedure using solid decaborane to make aluminum nanoparticles. This avoids some of the hazards of working with the highly toxic and pyrophoric diborane and pentaborane molecules.

Utah/UCLA publications resulting from this project.

1. Zandkarimi, B.; Alexandrova, A. N. Sn Content in Silica-Supported Pt_4Sn_x Model Catalysts as a Lever of Design for Selectivity of Dehydrogenation. **2019**, *in preparation*.
2. Gorey, T. J.; Zandkarimi, B.; Li, G.; Baxter, E. T.; Alexandrova, A. N.; Anderson, S. L. Oxide-supported Pt_nSn_x (n = 4, 7, 24) Model Catalysts: Coking Resistance in Dehydrogenation Chemistry via a New Mechanism. **2019**, *in preparation*.
3. Zandkarimi, B.; Gorey, T. J.; Li, G.; Baxter, E. T.; Anderson, S. L.; Alexandrova, A. N. Electronic effects leading to sintering suppression in size-controlled $PtSn/SiO_2$ bimetallic model catalysts. **2019**, *in preparation*.
4. Gorey, T. J.; Li, G.; Baxter, E. T.; Zandkarimi, B.; Alexandrova, A. N.; Anderson, S. L. Preparation of Size and Composition-controlled Pt_nSn_x/SiO_2 (n = 2, 4, 24) Bimetallic Model Catalysts using Atomic Layer Deposition. **2019**, *under review in J. Phys. Chem. C*.
5. Zandkarimi, B.; Alexandrova, A. N. Surface-supported cluster catalysis: ensembles of metastable states run the show. *WIRES* **2019**, *accepted*.
6. Halder, A.; Ha, M.-A.; Zhai, H.; B., Y.; Pellin, M. J.; Seifert, S.; Vajda, S.; Alexandrova, A. N., Switching Selectivity in the Oxidative Dehydrogenation of Cyclohexane on Subnanometer Palladium and Copper Clusters. **2019**, *under revision for ACS Catal*.
7. Jimenez-Izal, E.; Liu, J.-Y.; Alexandrova, A. N. Germanium as key dopant to boost the catalytic performance of platinum for alkane dehydrogenation. *J. Catal*. **2019**, *374*, 93-100
8. Jimenez-Izal, E.; Gates, B.; Alexandrova, A. N. The messy story of clusters in catalysis. *Phys. Today,* **2019**, *accepted*.
9. Zandkarimi, B.; Alexandrova, A. N. Dynamics of subnanometer Pt clusters can break the scaling relationships in catalysis. *J. Phys. Chem. Lett.* **2019**, *10*, 460-467.
10. Jimenez-Izal, E.; Zhai, H.; Alexandrova, A. N. Nanoalloying MgO-Deposited Pt Clusters with Si for Controlling the Selectivity of Alkane Dehydrogenation. *ACS Catal.* **2018**, *8*, 8346–8356.

11. Jimenez-Izal, E.; Alexandrova, A. N. Computational design of clusters for catalysis. *Ann. Rev. Chem. Phys.* **2018**, *69,* 377-400.
12. Jiang Yu; Jensen, Tonya N.; Lewis, William K.; Bunker, Christopher E.; Kelley, Steven P.; Rogers, Robin D.; Pryor, Owen M.; Chambreau, Steven D.; Vaghjiani, Ghanshyam L.; Anderson, Scott L.; Combustion Behavior of High Energy Density Borane-Aluminum Nanoparticles in Hypergolic Ionic Liquids, *Energy and Fuels*, **2018**, 32 (7), pp 7898–7908.
13. Zhai, H.; Alexandrova, A. N. Local Fluxionality of Surface-Deposited Cluster Catalysts: the Case of Pt_7 on Al_2O_3. *J. Phys. Chem. Lett.* **2018**, *9*, 1696-1702.
14. Baxter, E. T.; Ha, M.-A.; Cass, A. C.; Zhai, H.; Alexandrova, A. N.; Anderson, S. L., Diborane Interactions with Pt_7/Alumina: Preparation of Size-Controlled Boronated Pt Model Catalysts with Improved Coking Resistance. *J. Phys. Chem. C* **2018**, *122*, 1631-1644. DOI: 10.1021/acs.jpcc.7b10423
15. Zhai, H.; Alexandrova, A. N., Fluxionality of Catalytic Clusters: When It Matters and How to Address It. *ACS Catal.* **2017**, *7*, 1905-1911. DOI: 10.1021/acscatal.6b03243
16. Dai, Yang; Gorey, Timothy J.; Anderson, Scott L.; Lee, Sungsik; Lee, Sungwon; Seifert, Soenke; Winans, Randall E.; Inherent Size Effects on XANES of Nanometer Metal Clusters: Size-Selected Platinum Clusters on Silica", *J. Phys Chem. C* 121 (2017) 361-374
17. Ha, M.-A.; Baxter, E. T.; Cass, A. C.; Anderson, S.L.; Alexandrova, A. N., Boron Switch for Selectivity of Catalytic Dehydrogenation on Size-Selected Pt Clusters on Al_2O_3. *J. Am. Chem. Soc.* **2017**, *139*, 11568-11575. DOI: 10.1021/jacs.7b05894
18. Baxter, E. T.; Ha, M.-A.; Cass, A. C.; Alexandrova, A. N.; Anderson, S. L. Ethylene Dehydrogenation on $Pt_{4,7,8}$ clusters on Al_2O_3: Strong Cluster-Size Dependence Linked to Preferred Catalyst Morphologies. *ACS Catal.* **2017**, *7,* 3322−3335.
19. Zhai, H.; Alexandrova, A. N. Ensemble-Average Representation of Pt clusters in Conditions of Catalysis Accessed through GPU Accelerated Deep Neural Network Fitting Global Optimization. *J. Chem. Theor. Comput*. **2016**, *12*, 6213–6226.
20. Yu, Jiang; Boatz, Jerry A.; Anderson, Scott L.; Borane-Aluminum Surface Interactions: Enhanced Fracturing and Generation of Boron-Aluminum Core-Shell Nanoparticles, *J. Phys. Chem. C* 121, **(2017)** 14176–14190
21. Zhang, X.; Ganrefoer, G.; Alexandrova, A. N.; Bowen, K. Photoelectron Spectroscopic and Computational Study of the $PtMgH_{3,5}^-$ Cluster Anions. *Phys. Chem. Chem. Phys*. **2016**, *18*, 19345-19349.
22. Yu, Jiang; McMahon, Brandon; Boatz, Jerry A; Anderson, Scott L.; Aluminum Nanoparticle Production by Acetonitrile-Assisted Milling: The Effects of Liquid vs. Vapor Phase Milling, and

of Milling Method on Particle Size and Surface Chemistry. *J. Phys. Chem. C* 120 (2016), 19613–19629

People supported by this grant at UCLA:

Mai-Anh Ha (Ph.D. 2017),

Huanchen Zhai,

Borna Zandkarimi,

Dr. Elisa Jimenez-Izal.

People supported by this grant at U of Utah:

Yang Dai (Ph.D. 2017)

Eric T. Baxter (Ph.D. 2018)

Ashley C. Cass

Timothy J. Gorey

Guangjing Li

References Cited

1. Yeh, Y.-H.; Tsai, C.-E.; Wang, C.; Gorte, R. J., Heat-Flow Measurements for n-Hexane Reactions on H-ZSM-5 and H(Zn)-ZSM-5: Implications for Endothermic Reforming in Hypersonic Aircraft. *Ind. Eng. Chem. Res.* **2017,** *56* (21), 6198-6203.

2. Peng, Z.; Somodi, F.; Helveg, S.; Kisielowski, C.; Specht, P.; Bell, A. T., High-resolution in situ and ex situ TEM studies on graphene formation and growth on Pt nanoparticles. *Journal of catalysis* **2012,** *286*, 22-29.

3. Vu, B. K.; Song, M. B.; Ahn, I. Y.; Suh, Y.-W.; Suh, D. J.; Kim, J. S.; Shin, E. W., Location and structure of coke generated over Pt–Sn/Al2O3 in propane dehydrogenation. *Journal of industrial and engineering chemistry* **2011,** *17* (1), 71-76.

4. Burch, R.; Garla, L., Platinum-tin reforming catalysts: II. Activity and selectivity in hydrocarbon reactions. *Journal of Catalysis* **1981,** *71* (2), 360-372.

5. Lu, J.; Fu, B.; Kung, M. C.; Xiao, G.; Elam, J. W.; Kung, H. H.; Stair, P. C., Coking- and Sintering-Resistant Palladium Catalysts Achieved Through Atomic Layer Deposition. *Science* **2012,** *335* (6073), 1205.

6. Watwe, R. M.; Cortright, R. D.; Mavrikakis, M.; Nørskov, J. K.; Dumesic, J. A., Density functional theory studies of the adsorption of ethylene and oxygen on Pt (111) and Pt 3 Sn (111). *The Journal of Chemical Physics* **2001,** *114* (10), 4663-4668.

7. Gerceker, D.; Motagamwala, A. H.; Rivera-Dones, K. R.; Miller, J. B.; Huber, G. W.; Mavrikakis, M.; Dumesic, J. A., Methane Conversion to Ethylene and Aromatics on PtSn Catalysts. *ACS Catalysis* **2017,** *7* (3), 2088-2100.

8. Bednarova, L.; Lyman, C. E.; Rytter, E.; Holmen, A., Effect of Support on the Size and Composition of Highly Dispersed Pt–Sn Particles. *Journal of Catalysis* **2002,** *211* (2), 335-346.

9. Liu, S.; Dong, Q., Unique promotion effect of CO and CO 2 on the catalytic stability for benzene and naphthalene production from methane on Mo/HZSM-5 catalysts. *Chemical communications* **1998,** (11), 1217-1218.

10. Solymosi, F.; Erdöhelyi, A.; Szöke, A., Dehydrogenation of methane on supported molybdenum oxides. Formation of benzene from methane. *Catalysis Letters* **1995,** *32* (1-2), 43-53.

11. Ohnishi, R.; Liu, S.; Dong, Q.; Wang, L.; Ichikawa, M., Catalytic dehydrocondensation of methane with CO and CO2toward benzene and naphthalene on Mo/HZSM-5 and Fe/Co-modified Mo/HZSM-5. *Journal of Catalysis* **1999,** *182* (1), 92-103.

12. Fila, V.; Bernauer, M.; Bernauer, B.; Sobalik, Z., Effect of addition of a second metal in Mo/ZSM-5 catalyst for methane aromatization reaction under elevated pressures. *Catalysis Today* **2015,** *256*, 269-275.

13. Baxter, E., T.; Ha, M.-A.; Alexandrova, A.; Anderson, S. L., Ethylene Dehydrogenation on $Pt_{4,7,8}$ Clusters on Al_2O_3: Strong Cluster-Size Dependence Linked to Preferred Catalyst Morphologies. *ACS Catal.* **2017,** *7*, 3322-3335.

14. Dadras, J.; Jimenez-Izal, E.; Alexandrova, A. N., Alloying Pt Sub-nano-clusters with Boron: Sintering Preventative and Coke Antagonist? *ACS Catalysis* **2015**, 5719-5727.